Advanced Physics Lab II

Lab Report #1

Faraday and Kerr Effect

Group 1
Noah Horne, Luka Burduli

04/03/2025

Dr. Arnulf Materny
Dr. Faezeh Mohaghegh

We hereby declare that we (Luka Burduli and Noah Horne) are the sole authors of this lab report and have not used any sources other than those listed in the bibliography and identified as references throughout the report.

_____ _____

Contents

1 Abstract

The Faraday and Kerr effect are optical phenomena which occur primarily in gyromagnetic and transparent optically dielectric materials respectively. The Faraday effect refers to the induced chirality of a medium due to an incident magnetic field, causing incident linearly polarized waves to rotate themselves with an angle proportional to the mean magnetic flux density across the gyromagnetic sample. The Kerr effect on the latter, refers to the induced birefringency of specific optically dielectric materials when exposed to an incident perpendicular electric field. Associated to both effects are their respective constants, the Verdet Constant (V) and Kerr Constant (K) of the medium for the Faraday and Kerr effects respectively. During this experiment, the Verdet constants of a flint glass cylinder were calculated to be:

$$V_{440} = 51.59 \pm 2.04[radT^{-1}m^{-1}] \tag{1.1}$$
$$V_{505} = 31.44 \pm 2.63[radT^{-1}m^{-1}] \tag{1.2}$$
$$V_{525} = 30.96 \pm 1.14[radT^{-1}m^{-1}] \tag{1.3}$$
$$V_{580} = 24.96 \pm 1.51[radT^{-1}m^{-1}] \tag{1.4}$$
$$V_{595} = 21.6 \pm 0.52[radT^{-1}m^{-1}] \tag{1.5}$$

and the Kerr constant of a PLZT element was calculated to be $(9.13 \pm 0.25) \cdot 10^{-10} m/V^2$. All collected values sufficiently adhere to their respective literary counterparts.

2 Introduction & Theory

This investigation focuses primarily on the quantitative analysis of the Faraday and Kerr effects, together with the subsequent calculation of the Verdet and Kerr constants of a flint glass cylinder and a PLZT Kerr element, respectively. Both of these effects are applied practically to modulate light at high frequencies due to the lack of a time delay modifying light. The Faraday effect, more specifically the magneto-optic Faraday effect, concerns the induced optical activity of an optically dielectric medium due to a parallel magnetic field. As a polarized electromagnetic wave passes through such an exposed optically dielectric medium, its axis of polarization is rotated throughout its propagation through the material and emerges linearly polarized along a rotated axis. If then measured against an analyzer, the precise angle of rotation due to the Faraday effect can be observed.

One can describe the optical rotation of a polarized electromagnetic wave through the circular birefringence exhibited by the optically dielectric medium, causing left and right circularly polarized electromagnetic waves to traverse the dielectric material at differing wave speeds. As a result, however, when a linearly polarized wave enters such a medium, a superposition of these two effects occurs, causing the axis of polarization to rotate along a direction dictated by

said superposition. The stronger the mean magnetic flux density $\overline{B}$ about the optically dielectric flint glass sample, the greater its chirality—causing the angular displacement of the polarized wave to increase proportionally. For a specific wavelength of light, the angular displacement ϕ of a polarized electromagnetic wave's polarization axis is dictated by the following formula:

$$\Delta\phi = Vl\overline{B} \tag{2.1}$$

Where in equation 2.1, l is the optical path length of the flint glass sample—approximately 30mm—and V is called the Verdet constant with unit $[\frac{rad}{Tm}]$. However, the formula above is limited in its application to fixed wavelengths, as the Verdet constant varies with respect to the wavelength λ of incident light. As one may recall from Optical Physics, the refractive index of a medium is wavelength dependent due to chromatic dispersion. Similarly, the angular displacement of the light waves is dependent on the induced circular birefringence of the medium and in turn the refractive index n. For this reason, the Verdet constant wavelength dependence V can be expressed as proportional to the product of the wavelength and the wavelength dependence of the medium used.

$$V = V'\lambda\frac{dn}{d\lambda} \tag{2.2}$$

Here, V' is the fixed proportionality constant relating the Verdet constant V to the wavelength and refractive index change λ and $\frac{dn}{d\lambda}$ respectively. As one can infer from formula 2.2, in wavelength neighborhoods such that the change in refractive index with respect to the change in wavelength is quite large, the Verdet constant increases. This class of behavior is commonly observed for wavelengths close to the spectral lines of the medium.

In practice, the linear relationship between the mean magnetic flux density across the sample $\overline{B}$ and the resultant angular displacement $\Delta\phi$ is observed, and the Verdet constant determined. However, one must first define and calculate the mean magnetic flux density across the sample for a given current. As the magnetic field is not directly measured, it would be beneficial to first establish a concrete relationship between the current through the used electromagnetic coils and the magnetic field experienced by the sample. To do so, the change in magnetic flux density with respect to position in the sample is measured and numerically integrated to obtain the mean value for several fixed currents I between 0.5A and 4A. As a linear interpolation method is used to create the functional approximation of the shape of the magnetic field, the trapezoidal integration scheme is most appropriate. The discrete trapezoidal integral approximation for a position dependent discrete function $f(x_i)$ is given by:

$$A_N = \sum_{i=1}^{N}\left[\frac{1}{2}(f(x_{i+1}) + f(x_i))\Delta x\right], \quad \Delta x = \frac{x_n - x_1}{N} \tag{2.3}$$

To find the mean flux density $\overline{B}$ for a given integral over position of the magnetic flux $B(x_i)$, one simply divides the integral approximation 2.3 by the length of the interval used $x_n - x_0$, e.g:

$$\overline{B} = \frac{1}{x_n - x_1} \sum_{i=1}^{N-1} \left[\frac{1}{2} (B(x_{i+1}) + B(x_i)) \Delta x \right] \tag{2.4}$$

After calculating the mean flux density $\overline{B}$ for 6 different currents I, the relationship between the magnetic flux density and the current through the electromagnetic coils is plotted. It is expected from electromagnetism that the relationship between the current through a coil and the resultant magnetic field inside of it is given by the formula:

$$B = \mu_0 \cdot \mu_r \cdot \frac{I \cdot n}{l} \tag{2.5}$$

where μ_0 and μ_r are the magnetic permeability of free space and the relative magnetic permeability of the core used, respectively, l is the length of the solenoid, and n is the number of turns in the coil. As this equation describes the magnetic field in the center of a solenoid, it may be appropriate then to extend this linear relationship in some way to the superposition of the magnetic fields right above two copper coils. While it will not be exactly the same due to the decay of the magnetic field, this equation allows us to predict that the relationship between current and magnetic field will be linear. With such a linear relationship, one will be able to accurately predict the mean magnetic flux density given a measured current across the coils. This conversion between current and mean magnetic flux density $\overline{B}$ is imperative to the analysis of the Faraday effect, as the slope of the graph obtained by plotting equation 2.1 and extracting the Verdet Constant.

While the Faraday effect examines the effect of induced circular birefringence and optical activity on incident light, the latter Kerr effect analyzes the effects of an orthogonal electric field to the plane of incidence inducing linear birefringence on a Kerr cell. In the context of this experiment, an electric field is produced through the application of a potential difference between two electrodes diametrically opposing one another across a Kerr cell.

Typical Kerr cells require that their molecular structure is of the form of a dipole. When this particular class of substance is exposed to an electric field, the dipoles orient themselves along the electric field, causing the molecular structure to become birefringent. The greater the electric field, the greater the consequent difference of refractive indices in this induced birefringent medium. When a linearly polarized beam of light is incident on this birefringent material, the light becomes circularly polarized due to the difference of refractive indices—ordinary n_o and extraordinary n_{eo}—as a path difference for each of the projections is introduced. This path difference can be described as the difference of the two refractive indices used Δn, which is concomitantly proportional to the square of the electric field E^2 for fixed wavelength λ:

$$\Delta n = n_{eo} - n_o = \lambda K E^2, \quad E = \frac{U}{d} \tag{2.6}$$

where K is the Kerr constant of the Kerr cell, U is the voltage across the electrodes in the Kerr cell, and d is the inter-electrode distance. This path difference 2.6 can be similarly expressed as a phase difference Δ through a simple linear transformation:

$$\Delta = 2\pi\frac{l}{\lambda}(\Delta n) = 2\pi K l E^2, \quad E = \frac{U}{d} \tag{2.7}$$

Where l is the distance travelled by the light through the Kerr element. In practice, light is first linearly polarized with a polarization axis 45 degrees to the direction of the electric field. As the light passes through the Kerr cell, the phase difference Δ is introduced. Depending on this phase difference, the emergent light takes on a specific elliptical polarization. The light emerges circularly polarized only when $\Delta = \frac{\pi}{2}$, linearly polarized when $\Delta = m\pi, m \in \mathbb{N}$, and elliptically polarized otherwise. This emergent light is then incident on an analyzer which is perpendicular to the initial polarizer such that if $\Delta = 2m\pi, m \in \mathbb{N} \cup \{0\}$, then no light passes through the final analyzer. Applying Malus' Law, it is known that the intensity I of the emergent light from the analyzer is formulaically expressed as:

$$I = I_0 \cos^2(\frac{\pi + \Delta}{2}) = I_0 \sin^2(\frac{\Delta}{2}) \tag{2.8}$$

where I_0 is the intensity with no electric field applied and a difference of 0 radians between the polarizer and analyzer. In a sense, it is the maximum possible intensity to which one can normalize all results. Notice that when the phase difference Δ is π, a maximum in the intensity is observed. This is because the light emerges from the Kerr cell linearly polarized, but rotated by $\frac{\pi}{2}$, precisely aligning with the optical axis of the analyzer.

As the electric field E is unknown experimentally, it is not possible to apply equation 2.7 to find the phase difference. Alternatively, it may be beneficial to rearrange Malus' law 2.8 to find the phase difference Δ in terms of the intensity I, I_0 (measurable quantities). Rearranging equation 2.8, one achieves:

$$\Delta = 2\arcsin\sqrt{\frac{I}{I_0}} \tag{2.9}$$

Substituting equation 2.9 into equation 2.7, one can construct a relationship between the voltage across the electrodes and the intensity measured after the analyzer.

$$2\arcsin\sqrt{\frac{I}{I_0}} = \frac{2\pi K l U^2}{d^2} \tag{2.10}$$

$$U^2 = \frac{d^2}{\pi K l} \cdot \arcsin\sqrt{\frac{I}{I_0}} \tag{2.11}$$

The equation above is the main equation used to determine the Kerr constant of the Kerr cell for this investigation. By plotting the square of the voltage across the Kerr cell U^2 electrodes against $\arcsin\sqrt{\frac{I}{I_0}}$, the Kerr constant K can be easily extracted from the slope $\frac{d^2}{\pi K l}$.

3 Setup & Experimental Procedure

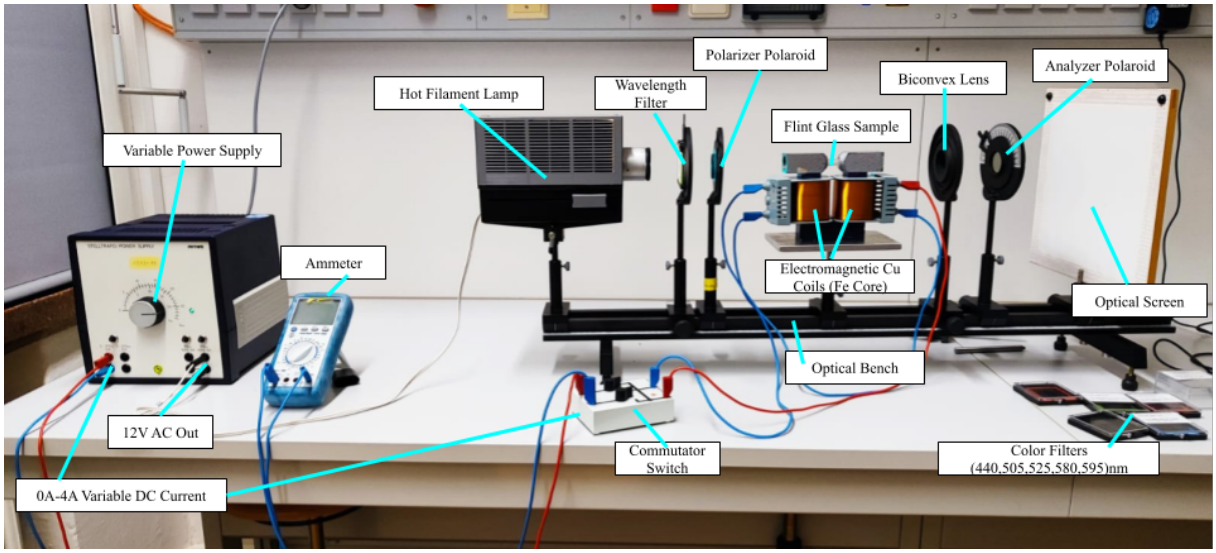

Figure 1: Annotated Experimental Setup for Faraday Effect Investigation

The experimental setup for the investigation of the Faraday Effect positions a linearly polarized monochromatic light beam incident on a Flind Glass Sample exposed to a magnetic field. As the light travels through this optically dielectric material, the circular birefringence induced in the flint glass rotates the light beam, causing the intensity of light which makes it through the analyzer to drop. As seen in Figure 1, a hot filament lamp supplied with 12 Volt AC output is used as a light source. Initially, the polarizer Polaroid and analyzer Polaroid are positioned such that their optical axes lie parallel to one another–such that an intensity maximum is observed on the white optical screen behind the analyzer. As the magnetic flux is varied across the Flint Glass Sample–positioned above the two electromagnetic copper coils seen in the figure–the intensity of the incident light to the optical screen will decrease, as the emergent light will no longer be parallel to the analyzer's optical axis. To measure the rotation angle, the analyzer axis is rotated such that a maximum intensity is observed. Then, with the same current and wavelength, the commutator connected to the coils is switched, reversing the direction and consequent optical activity of the flint glass sample. The analyzer Polaroid is again rotated in the opposite direction such that a new maximum is observed, and the difference of the two angles measured as $2\Delta\phi$.

The data collected throughout this experiment makes use of 6 different wavelength filters–440nm, 505nm, 525nm, 580nm, 595nm–for which each is examined across 6 different current values–0.5A, 1.0A, 1.5A, 2.0A, 3.0A, 4.0A respectively–resulting in 6 different mean magnetic flux densities $\overline{B}$ per wavelength across the sample. Using the relationship between the measured angle of rotation $\Delta\phi$ and the mean magnetic flux density across the sample $\overline{B}$, the Verdet Constant V for each of the 6 wavelengths λ is determined by applying formula 2.1.

The aforementioned process concerns the bulk of the experimentally significant data

collected during this experiment. However, one must still perform some preparatory work to determine the relationship between the current through the electromagnetic coils and the mean magnetic flux density. To calculate the mean magnetic flux density across the sample, a magnetic probe was moved in steps of 5mm through the cavity where the sample would lie such that a clear plot of the magnetic flux with respect to position was made. Using this plot, the points were numerically interpolated to form a piecewise linear graph, which was then trapezoidally integrated to calculate the mean magnetic flux density, as denoted in formula 2.4. This process was repeated for currents 0.5A, 1A, 1.5A, 2A, 3A and 4A, such that a linear relationship between the mean magnetic flux density and the current across the electromagnetic coils could be plotted, and consequently used for the remainder of the investigation.

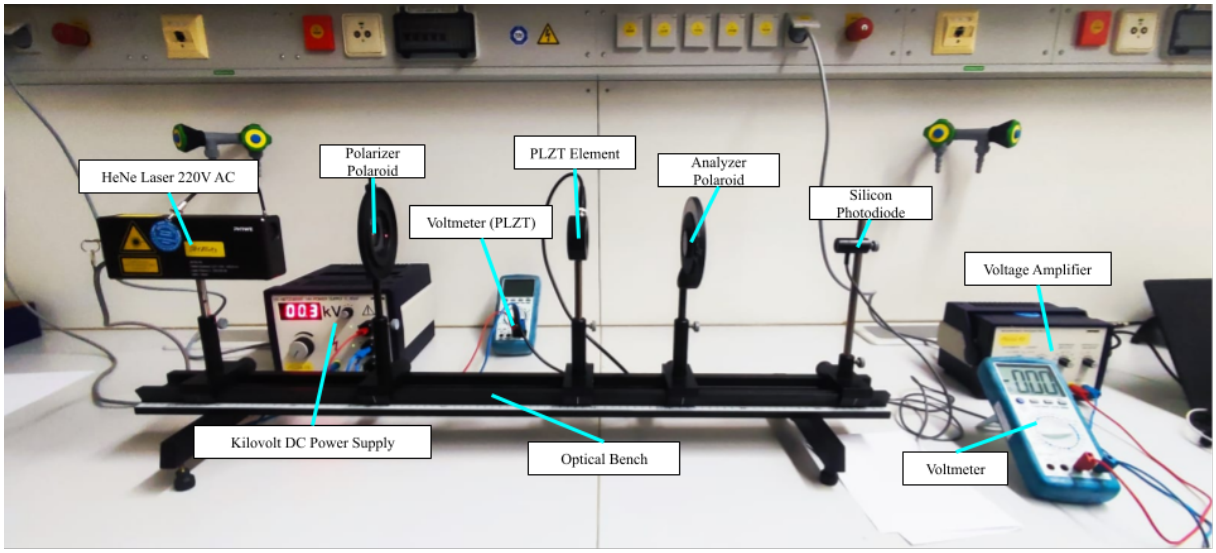

Figure 2: Annotated Experimental Setup for the Kerr Effect Investigation

The experimental setup for the investigation of the Kerr effect makes use of a polarized Helium-Neon (He-Ne) laser incident on a PLZT element (Lead-Lanthanum-Zirconium-Titanium compound). The PLZT element is positioned such that it lies between two diametrically opposed electrodes which respectively produce an incident electric field perpendicular to the optical axis of the incident light. As the laser used is a gas laser (He-Ne) it was crucial that it was allowed one hour to stabilize its signal and reach equilibrium such that a consistent output intensity was measured. Due to the dipole-like structure of the PLZT compound, an incident electric field causes the molecules to orient themselves such that the Kerr cell exhibits an induced birefringency. After emerging from the Kerr cell, the light–now elliptically polarized with some phase difference dependent on the square of the electric field E^2–is incident to an analyzer polaroid positioned at $90°$ to the initial polarizer. The transmitted intensity is then measured as an amplified voltage V by a silicon photodiode. As one can observe in figure 2 above, the PLZT element is connected to a variable power supply to allow the convenient manipulation of the potential

difference across the diametrically opposed electrodes (integrated in the PLZT element).

To begin the experiment, the maximum transmitted intensity with zero electric field–I_0 in formula 2.9–must first be measured to serve as a normalization constant in our trend line, and to help calculate the phase difference due to the birefringency of the PLZT element. This is measured by first fixing the angle of the polarizer and analyzer to be equal, and measuring the resultant amplified voltage of the photodiode. After this measurement is taken, it is used for all consequent calculations of the phase difference as I_0.

After I_0 is found, the first polarizer is rotated such that its polarization axis lies at a 45° angle to the ordinary and extraordinary polarization axis of the PLZT element, and the analyzer is rotated such that it lies perpendicular to the initial analyzer. After the optical bench is set up according to the aforementioned steps, the voltage across the PLZT element is varied from 90V to 1150V, and the resultant voltage of the silicon photodiode measured. Using the ratio of voltages the same way as the ratio of intensities (as they are directly proportional), one can consequently apply formula 2.9 to compute the phase difference. With this phase difference, one can plot the relationship between the squared applied voltage to the PLZT element and the phase shift of the laser. This result will be linear, and follow the behavior dictated by formula 2.11. Extracting the Kerr constant from the slope is then performed through a simple term rearrangement.

4 Results and Data Analysis

4.1 Investigation of the Faraday Effect

To investigate the Faraday effect, one first must determine the relationship between the applied current to the electromagnetic copper (Cu) coils, and the mean magnetic flux density across the flint glass sample. To do so, the relationship between the measured flux density with respect to position was measured for currents between 0.5A and 4.0A. The positions were varied with a step width of 5mm such that a sufficient resolution of the resultant magnetic field density could be observed. For each current through the electromagnetic coils 7 magnetic flux density measurements were taken corresponding to positions from 0mm to 30mm respectively. It is also important to note that the reference point of the position was taken to be the very beginning of the flint glass cavity, such that a position of 0mm corresponds to the hall probe at one of the ends of the sample cavity. These results were then promptly tabulated into tables such as the one displayed below. For sake of a clean visualization and lack of clutter, only one of the tables from the 6 currents measured is displayed inline. For details regarding the rest of the tables, please consult Appendix 8.1.

Table 1: Measurements for Coil Current 3.0A	
Position $(mm) \pm 0.5mm$	Magnetic Flux Density $(T) \pm (10^{-4})$
0	0.0363
5	0.1376
10	0.1911
15	0.1922
20	0.1741
25	0.0896
30	0.0097

The plot for the tabulated data of flux density (T) with respect to the Hall probe position (mm) for coil current 3A is displayed in the graph below. All other plots for further current values can be observed similarly in Appendix 8.1. Once the tabulated data was collected, a linear interpolation of the plots was constructed as a best estimate for the magnetic flux density curve. Using a self-designed Python script coupled with numerical integration methods, the interpolated curve was trapezoidally integrated along a discrete partition corresponding to the data obtained during the measurement for a fixed current. This integral value was then used in conjunction with formula 2.4 to estimate the mean flux density (displayed as a red horizontal line in Figure 3 below).

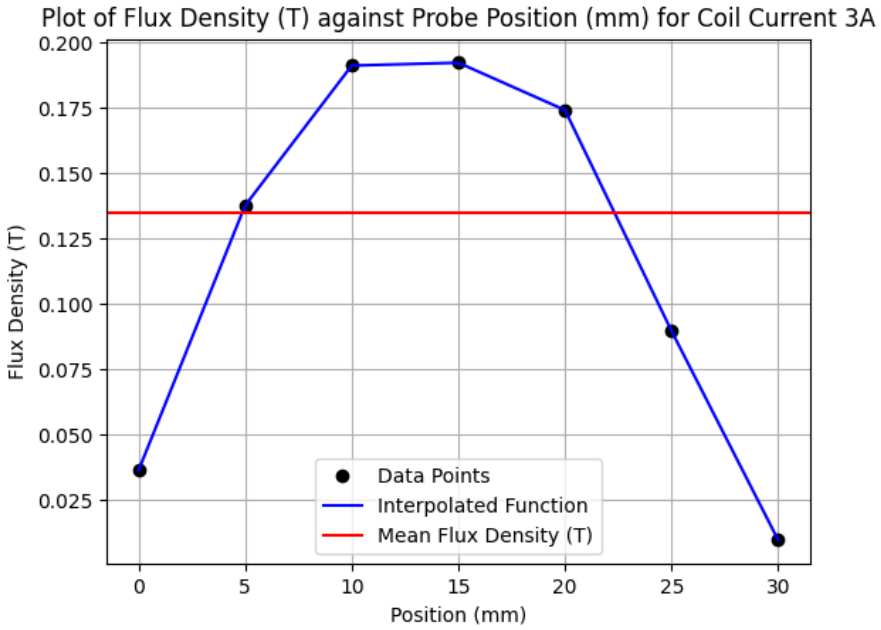

Figure 3: Plot of flux density (T) against probe (mm) for coil current 3 A

To better illustrate the method of trapezoidal integration for this example, a sample calculation of the mean magnetic flux density $\overline{B}$ will be written below. First one starts with formula 2.4, substituting the appropriate values from table 1.

$$
\begin{aligned}
\overline{B} &= \frac{1}{x_n - x_1} \sum_{i=1}^{N-1} \left[\frac{1}{2} (B(x_{i+1}) + B(x_i)) \Delta x \right] \\
&= \frac{1}{30} \sum_{i=1}^{N-1} \frac{5}{2} \left[(B(x_{i+1} + B(x_i)) \right] \\
&= \frac{1}{12} ((0.1376 + 0.0363) + (0.1911 + 0.1376) + (0.1922 + 0.1911) + \\
&(0.1741 + 0.1922) + (0.0896 + 0.1741) + (0.0097 + 0.0896)) \\
&= \frac{1}{12} (1.6152) \\
&= 0.1346[T]
\end{aligned}
$$

$$
\implies \overline{B} = 0.1346[T] \text{ for current 3A.} \tag{4.1}
$$

As one can see from the horizontal red line in figure 3, this is the exact value of the mean magnetic flux density $\overline{B}$ for a corresponding coil current of 3A through the copper coils below the flint glass sample. This same class of measurements and calculation was repeated for a range of currents between 0.5A and 4A, allowing one to properly analyze the relationship between the current through the electromagnetic coils and the mean magnetic flux density across the sample. As a means of more efficiently displaying the relative scaling for each current, a plot containing all the magnetic flux densities with respect to position along the sample cavity was created.

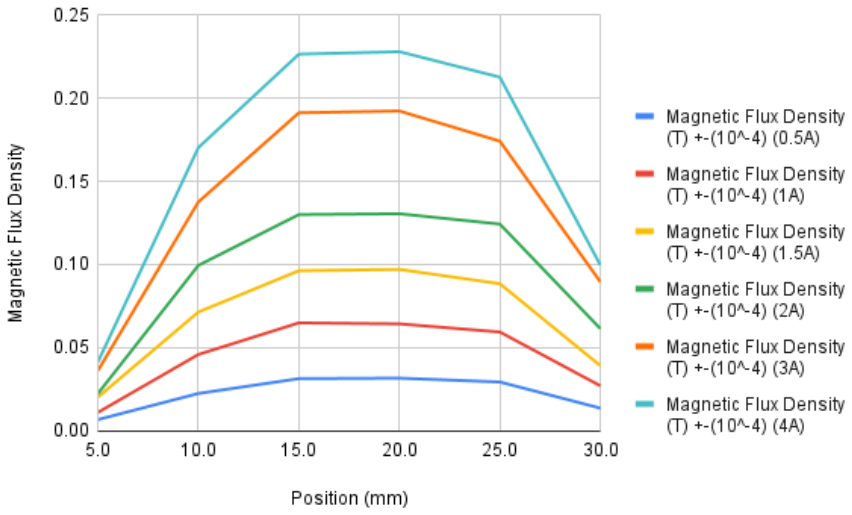

Figure 4: Plot of Magnetic Flux Density against Position (mm)

The plot above qualitatively demonstrates that as the current through the electromagnetic coils increases, the average magnetic flux density $\overline{B}$ increases proportionally. The curves exhibit a centralized distribution, which indicates that the highest magnetic flux density occurs near the center of the crystal. This makes sense due to the superposition mediating behavior of the B-field, the strongest flux density occurring at the position where the contributions from both electromagnetic coils sum together. While this plot demonstrates quite clearly that the average magnetic flux does indeed increase for an increasing current, it is lacking in the explicit visualization of this relationship. To better examine the relationship between current and mean magnetic flux density, a plot between the two values was made.

From the previously mentioned theory relating the current and magnetic field on the inside of a solenoid (formula 2.5, it can be expected that the relationship will follow linear behavior. Plotting the results for each mean magnetic flux density $\overline{B}$, it is clear from the plot below that a linear prediction is indeed observed.

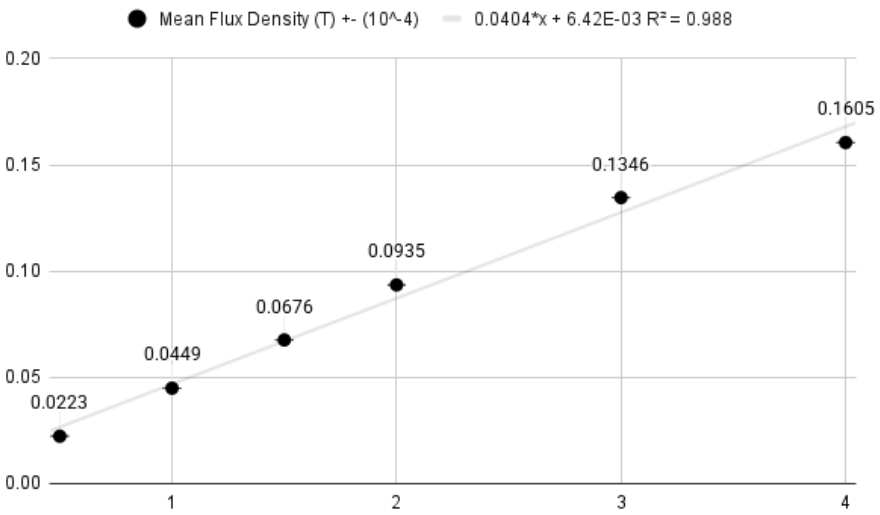

Figure 5: Plot of Mean Flux Density (T) against Coil Current (A)

Indeed, the plot of the mean flux density $\overline{B}$ against the coil current I exudes a directly proportional relationship between the two variables. By fitting a least squares linear regression to the data, the relationship between the two variables can be classified by the following relationship:

$$\overline{B} = 0.0404I + 6.42 \cdot 10^{-3} \tag{4.2}$$

In the obtained relationship, the absolute uncertainty of the slope is ± 0.0022. Since the measurements were taken in the gap between two coils rather than directly inside them, some deviations from the ideal proportionality is definitely expected. Despite this deviation due to alternative position, the graph confirms that the same linear relationship holds even outside the coils' centers, for a clearly positive directly proportional trend is observed between the coil current I and the mean magnetic flux density $\overline{B}$. Equation 7.1 can now be used to easily convert measurements of current to mean magnetic flux density without the need of manually computing the mean repeatedly.

To calculate Verdet's constant V, the rate of change of the angle deflection with respect to the mean magnetic flux density was measured. To do so, the polarizer was fixed at an angle of 45 degrees, and the analyzer was set to -45 degrees. Such a configuration resulted in a minimal transmitted intensity when the current across the magnetic coils was set to 0. The rotation of the plane of polarization was then measured for different coil currents using color filters which only transmitted a specific wavelength. As 5 different wavelengths were used–440nm, 505nm, 525nm, 580nm, and 595nm–only the results for $\lambda = 595nm$ are presented below for visual clarity. The results for other wavelengths can be found in Appendix 8.3. For currents ranging from 0 to 4.0A in steps of 0.5A (and in both the + and - direction by use of a commutator switch), the measured angles of rotation $2\Delta\phi$ were recorded, and the corresponding magnetic flux densities calculated using the previously determined relationship (equation 7.1). The results of these measurements are detailed in the table below.

Table 2: Coil Current (A) against $\Delta\phi$ for Wavelength 595nm

Coil Current (A) $\pm(0.1A)$	Ang 1 (+) $\pm(0.5\text{deg})$	Ang 2 (-) $\pm(0.5\text{deg})$	Difference $\Delta\phi$ $\pm(0.9 \cdot 10^{-2})$rad	Flux Density (T) $\pm(10^{-4})$
0.0	45	45	0.000	0.006
0.5	43	45	0.017	0.027
1.0	43	46	0.026	0.047
1.5	42	47	0.044	0.067
2.0	41	47	0.052	0.087
2.5	40	48	0.070	0.107
3.0	40	49	0.079	0.128
3.5	39	50	0.096	0.148
4.0	38	50	0.105	0.168

The data for $\lambda = 595nm$ in Table 2 demonstrates a clear increase in the rotation angle $\Delta\phi$ with increasing coil current, as expected from the Faraday effect. To specifically extract the Verdet constant for the a specific wavelength, the Verdet constant V is determined through the rearrangement of terms in the slope of equation 2.1. To do so, a linear relationship must be established between the mean magnetic flux density $\overline{B}$ and the angle of rotation. Below is the plot of the angle difference $\Delta\phi$ against the mean magnetic flux density $\overline{B}$.

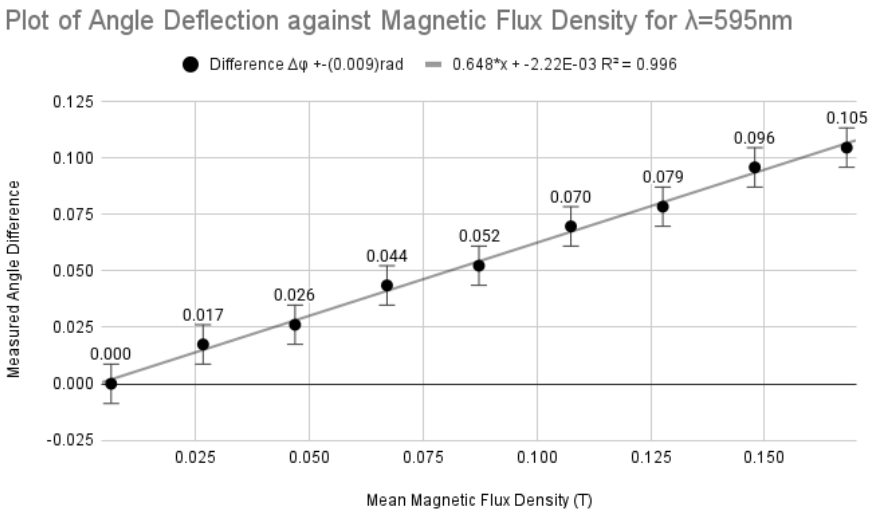

Figure 6: Plot of Angle Deflection $\Delta\phi$ against Magnetic Flux Density for $\lambda = 595nm$

For $\lambda = 595nm$, the extracted slope of the graph was found to be $0.6479 \pm 0.0157[radT^{-1}]$. Knowing the optical path length of the flint glass sample to be L=0.03[m] and making use of the equation 2.1, the Verdet constant V was found to be $V = 21.597 \pm 0.524$ through the following derivation.

$$\begin{aligned} \Delta\phi &= Vl\overline{B} \\ \implies Vl &= \text{slope} = 0.6479 \\ \implies V &= \frac{0.6479}{0.03} = 21.597 \pm 0.524[radT^{-1}m^{-1}] \end{aligned}$$

As with the previous section, the Verdet constants V for other wavelengths λ were determined through exactly similar calculations. The final values for the Verdet constant for wavelengths 440nm, 505nm, 525nm, 580nm, 595nm incident on a Flint glass sample were calculated through the aforementioned method to be:

$$V_{440} = 51.59 \pm 2.04[radT^{-1}m^{-1}] \tag{4.3}$$
$$V_{505} = 31.44 \pm 2.63[radT^{-1}m^{-1}] \tag{4.4}$$
$$V_{525} = 30.96 \pm 1.14[radT^{-1}m^{-1}] \tag{4.5}$$
$$V_{580} = 24.96 \pm 1.51[radT^{-1}m^{-1}] \tag{4.6}$$
$$V_{595} = 21.6 \pm 0.52[radT^{-1}m^{-1}] \tag{4.7}$$

After calculating the Verdet constant V, the constants were plotted with respect to the wavelength of each measurement series. It is predicted by the relevant aforementioned theory and equation 2.2 that the Verdet constant changes with respect to the wavelength of the incident

light in a nonlinear fashion. Below is the plot which demonstrates this behavior qualitatively and in an intuitive manner.

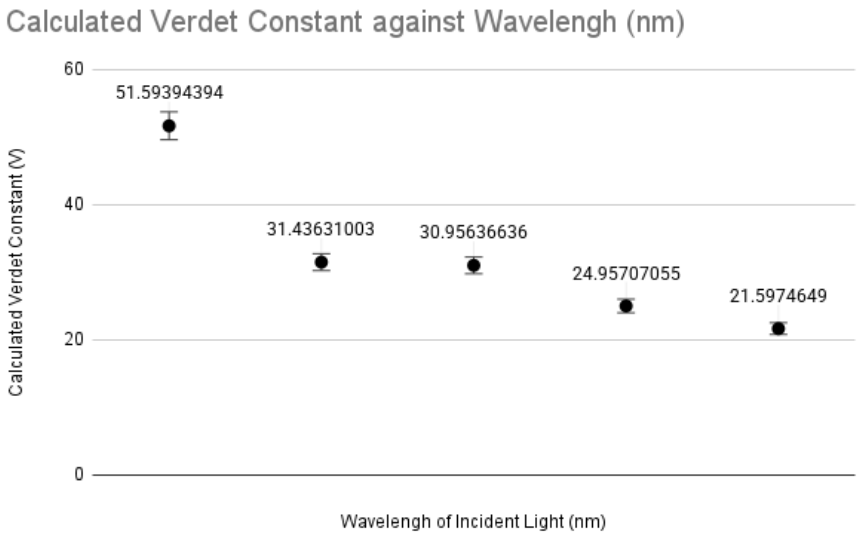

Figure 7: Plot of Calculated Verdet Constant vs. Wavelengh (m)

The graph below demonstrates a clear nonlinear inverse relationship between the Verdet Constant and the fixed wavelength of the incident light. As the wavelength of the light increases, the calculated Verdet constant can be seen to decrease. This indicates that for longer wavelengths, the rotation of light waves passing through an optically dielectric medium exposed to a magnetic field is significantly reduced. In practice, these results are adherent to the expected behavior of the the Faraday effect, as longer wavelengths exhibit larger phases which are in turn less affected by the rotational birefringency of the flint glass element.

4.2 Investigation of the Kerr Effect

The Kerr effect refers to an optical phenomena which occurs in specific transparent optically dielectric materials such as glass and plastic. When an optically dielectric material (also called a Kerr medium) is exposed to a perpendicular electric field its structure becomes electrically polarized and the molecular lattice becomes birefringent. The intensity of this incident electric field is directly related to the induced birefringency in the medium. As one can recall from birefringent theory, when linearly polarized light is incident at an angle to the extraordinary and ordinary axes of a birefringent medium, its wave path becomes circularly polarized dependent on the phase difference introduced by the birefringent element. When emerging from a birefringent medium, the waves can be either linearly polarized, having gone through a complete phase difference of a multiple of π radians, or elliptically polarized. Depending on the

exact phase difference introduced, the transmitted light behaves differently when incident on an analyzer. The closer the phase difference is to π, the brighter the transmitted intensity.

To investigate the Kerr effect, a Helium Neon (He-Ne) gas laser was used. Before the experiment began, the He-Ne laser was heated for an hour to ensure minimal signal fluctuations due to atmospheric noise. Once equilibrium was reached in the He-Ne laser, the maximum possible voltage measurement of the silicon photo diode U_0 given the optical configuration was measured as a normalization factor. To do so, the analyzer and polarizer were aligned such that their optical axes were parallel and the voltage across the Kerr cell was set to zero such that no phase difference was introduced.

After the normalization constant was measured, the measured intensity behind the analyzer was recorded in terms of voltage and was measured to be $U_0 = 4.42 \pm 0.01[V]$. To investigate the Kerr effect appropriately, the voltage applied to the PLZT element was varied from $90 \pm 0.01V$ to $1150 \pm 0.01V$ and the corresponding photodiode voltage was recorded. The measured photodiode voltage values were plotted against the applied voltage as shown in Figure 8.

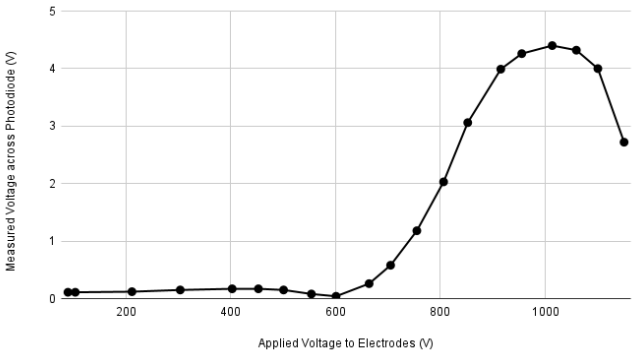

Figure 8: Plot of Measured Photodiode Voltage (V) against Applied Voltage (V) on the Electrodes

Further examining this data, it is clear that a maximum voltage is observed around a voltage of 1000V. The data has a skew centralized behavior which is characteristic of the Kerr effect. From voltages ranging from 0 to $600 \pm 0.01V$, the transmitted intensity remained relatively zero, which indicates minimal induced birefringence in the PLZT element. After $600 \pm 0.01V$ the intensity began to increase and exhibited the aforementioned peak around 1000 V. This behavior aligns with theoretical expectations, as it is likely that around the voltage of 1000V a phase difference of π radians is observed. If one observes the graph of the squared applied voltage against phase shift (Figure 10), one can see that this is indeed the case, and a phase difference of π radians approximately coincides with a voltage of 1000V. To further analyze the Kerr effect, the measured values were normalized with respect to the initial photodiode voltage U_0 and plotted against the applied voltage U.The table of these values can be seen below, and the respective plot of the data as well.

Table 4: the normalized Voltage vs. applied voltage.				
Normalized Voltage (V)	Normalized Voltage Error (V)	Applied Voltage (V) +-0.01	Phase Shift (Rad)	Phase Shift Error (Rad)
0.025	0.0023	90	0.317	0.0145
0.025	0.0023	104	0.317	0.0145
0.027	0.0023	212	0.331	0.0139
0.034	0.0023	304	0.371	0.0125
0.038	0.0023	403	0.395	0.0118
0.038	0.0023	453	0.395	0.0118
0.034	0.0023	501	0.371	0.0125
0.018	0.0023	554	0.270	0.0170
0.009	0.0023	601	0.191	0.0239
0.059	0.0023	664	0.490	0.0096
0.131	0.0023	705	0.741	0.0068
0.267	0.0023	755	1.086	0.0053
0.459	0.0025	806	1.489	0.0050
0.692	0.0028	852	1.966	0.0060
0.903	0.0030	915	2.507	0.0103
0.964	0.0031	955	2.759	0.0168
0.995	0.0032	1013	3.007	0.0476
0.977	0.0032	1059	3.444	0.0213
0.905	0.0031	1100	3.768	0.0104
0.615	0.0027	1150	4.480	0.0055

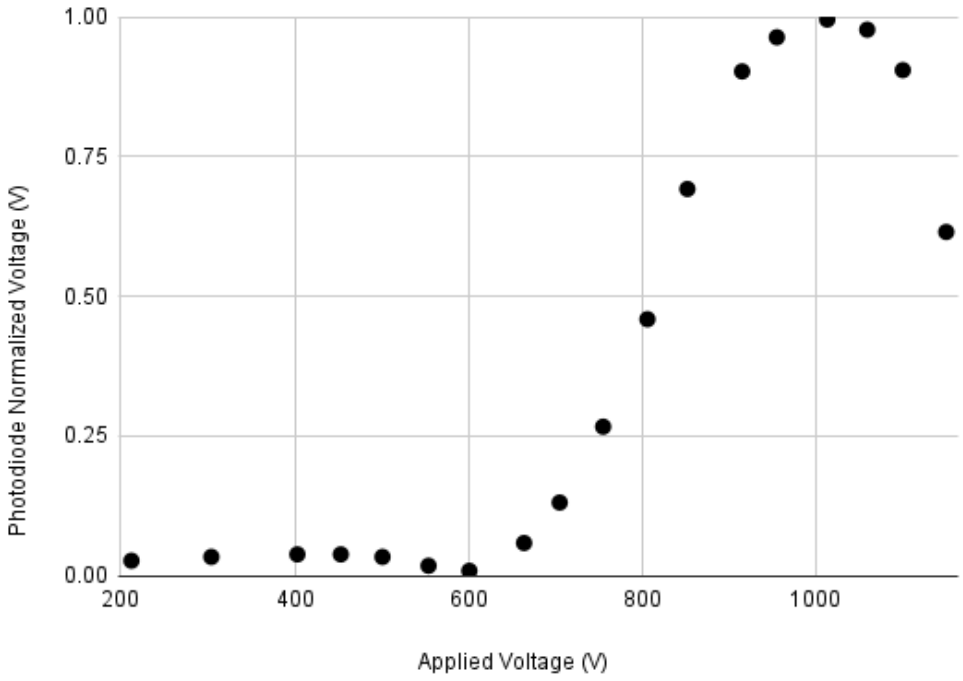

Figure 9: Plot of Photodiode Normalized Voltage(V) against Applied Voltage (V)

It can be seen that as the voltage increases the phase shift grows, which leads to the constructive interference. The intensity reaches a peak at $1013 \pm 0.01V$, where the phase shift should hits π. For phase differences which are greater than π, a phase correction of $2\pi - \Delta\phi$ was needed to to avoid the overflow of the arcsin function when applying equation 2.11.

To determine the Kerr constant, the squarerd applied voltage was plotted against the corresponding phase shift calculated through formula 2.7. This can be seen in Figure 11. According to the Kerr effect, a linear relationship between the square of the transmitted Voltage U^2 and the phase difference due to the Kerr cell $\Delta\phi$ should be observed. From the plot below, it is clear that this is indeed the case after the voltage is large enough to begin inducing birefringency in the material (occurs when $U^2 \approx 400000$).

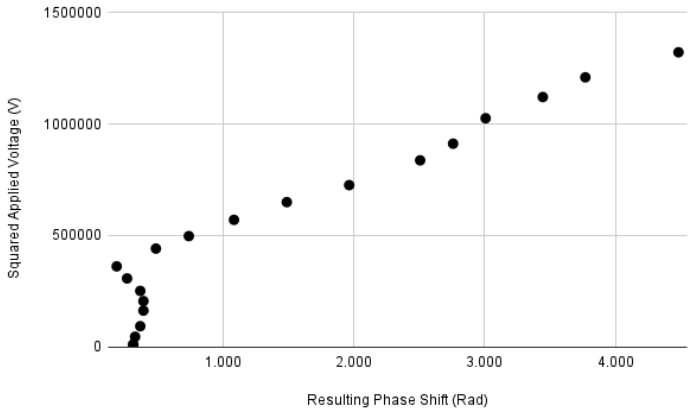

Figure 10: Plot of the Squared Applied Voltage (V^2) Against Resulting Phase shift (Rad)

From the data it can be immediately observed that for lower voltages (600V and below) no linear dependence is exhibited. This is due to the fact that the electric field generated by these voltages was not strong enough to induce a detectable change in refractive index. Beyond 600 V the phase shift behaves linearly with respect to V^2. For a correct calculation, only the domain of voltages which exhibited a linear relationship were used during the final calculations of the slope. After the domain was restricted, a linear regression was applied to the Squared Voltage against phase shift plot in order to extract the slope of the graph formulaically described by equation 2.11.

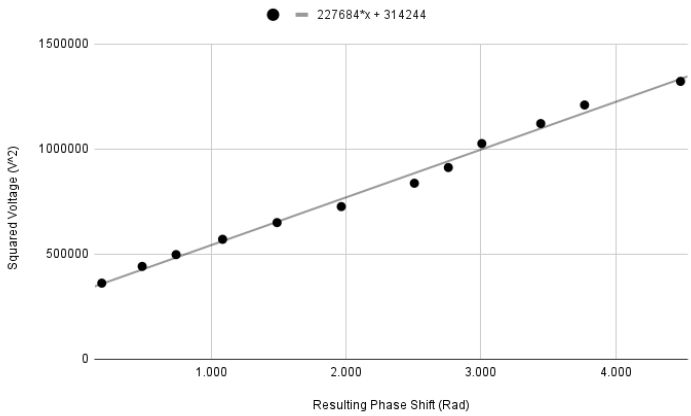

Figure 11: Plot of Squared Voltage (V^2) Against Resulting Phase Shift (Rad) (Linearly Behaving Part)

The slope of V^2 against $\Delta\phi$ was determined to be $m = 227684 \pm 6101[V^2 rad^{-1}]$. The Kerr constant was then calculated using the relation from equation 2.11:

$$K = \frac{d^2}{2lm\pi} \tag{4.8}$$

where d=0.0014m (width, distance between the electrodes) and l=0.0015m (length). The final value was obtained to be:

$$K = (9.13 \pm 0.25) \cdot 10^{-10} m/V^2$$

While the Kerr constant differs slightly from some of the theoretical values presented in the lab manual, it remains within a reasonable range considering the fact that the measured values depend on the history of the PLZT-element. This phenomena is directly stated as well in the Advanced Physics Lab II Manual (Materny & Mohaghegh, 2025).

5 Error Analysis

For all errors involving the slope of the graph, the uncertainty of the slope was approximated using the built-in function (LINEST), which works by approximating the linear slope of a set of data points through the least squares method. As a byproduct, the error of the slope is given in absolute form. Due to the efficiency of this method, and the large quantity of graphs, it was the clear choice for this investigation.

For all errors involving numerical calculations with propagated error, such as for the uncertainties of the final measurements of the Kerr Constant and Verdet Constants, the root sum of squares method (RSS) was employed. This method involves calculating the propagated error of a formulaic value by computing all partial derivatives with respect to all error-prone parameters, and taking it under a square root. The formula for this is given below.

$$\Delta y = \sqrt{\sum_{i=0}^{n} \left(\frac{\partial y}{\partial x_i} \cdot \Delta x_i \right)^2} = \sqrt{\left(\frac{\partial y}{\partial x_1} \cdot \Delta x_1 \right)^2 + \cdots + \left(\frac{\partial y}{\partial x_n} \cdot \Delta x_n \right)^2} \tag{5.1}$$

One major source of error in the determination of the magnetic flux density was the precision of the magnetic probe used for measurement. Additionally, as the probe was moved across the measurement positions, even minor misalignments or shifts in positioning could introduce a big range in the readings, particularly given the rapid decay of the magnetic field towards the edges of the crystal gap. The absolute error for the position measurement was 0.5mm (instrumental error), and for the voltage reading it was 0.01V. Furthermore, the instrumental error of the magnetic probe was 10^{-4} T.

In determining Verdet's constant, one of the primary sources of error was the mea-

surement of the rotation angle $2\Delta\phi$. Since the angle measurements were based on the human vision, human error in reading the minimum intensity could contribute to significant random inaccuracies, specifically for wavelengths on the boundary of human visibility. For the 440nm and 505nm wavelengths, the intensity of the transmitted light was within the visible range, however the smaller wavelengths were difficlt to make out on a white paper and did not transmit visibly. As a result, rather than using a paper optical backboard to observe the angle at which minimum intensity was reached, a direct visual observation through the analyzer was made. The uncertainty of the rotation angle was propagated into the final computation of Verdet's constant, leading to an associated error in the slope determination (calculated using LINEST function).

In regards to the Kerr effect, the presence of ambient light and variable background radiation may have also introduced small fluctuations in intensity readings. The instrumental error for the applied voltage was $\pm 1V$, and for the measured voltage it was $\pm 0.01V$. To propagate the uncertainty of the normalized intensity and phase shift, the standard propagation equation 5.1 was used:

$$\Delta I_n = I_n \sqrt{\left(\frac{\Delta I}{I}\right)^2 + \left(\frac{\Delta I_0}{I_0}\right)^2} \tag{5.2}$$

and

$$\Delta\theta_K = \frac{2}{\sqrt{1 - \left(\frac{I}{I_0}\right)^2}} \cdot \frac{1}{2}\left(\frac{1}{\sqrt{II_0}}\right)\Delta I \tag{5.3}$$

Similarly to calculate the Kerr constant equation 4.8 was used, however only the slope m carried the uncertainty $\Delta m = 6101$ (obtained from the LINEST function). In the end, the propagated error of the Kerr constant K is given by:

$$\Delta K = |\frac{-d^2}{2l\pi m^2}|\Delta m \tag{5.4}$$

Any noise in the intensity measurements, detector sensitivity issues, or slight misalignment in the experimental setup could have amplified this error. Also, it is worth mentioning that the measured values depend on the history of the PLZT-element as its previous states or exposures could affect the accuracy and consistency of the results.

6 Discussion

Reflecting on the investigation, it is evident that a thorough analysis of the optical properties of both materials, flint glass and PLZT element, Faraday and Kerr effects-was successfully investigated. The experiments provided valuable insights into the magneto- and electro-optical phenomena exhibited by the given materials.

In the Faraday effect, the relationship between magnetic flux density and coil current was investigated. Similarly, the Verdet's constant, determined for different wavelengths, followed expected trends, demonstrating the material's magneto-optical behavior. For the Kerr effect, the Kerr constant was derived for the PLZT element and the experimental data for squared voltage versus resulting phase shift performed a linear dependence. The methodology used in this investigation was mostly effective. However, there are areas in which the experimental design could be improved to improve the accuracy and precision. One such limitation could come from experimental uncertainties, such as measuring flux in the Faraday experiment.

The interpolation of the flux density with respect to position showcased clearly linear dependence as it was expected, however, error in the method could increase for higher currents (due to the bigger fluctuations in the magnetic field).In future experiments, it might be useful to use a more precise flux meter or employ a larger measurement interval to reduce errors due to the small variation in flux density at higher currents. Additionally, more careful control of the coil current would help ensure that the flux density calculations remain within the desired range.

Regarding the Verdet's constant, the decrease in the constant with increasing wavelength supports the theoretical dependence and validates the experimental method. However, the measurements were based on the visible range of the human eye, which decreases logarithmically. Using an optical sensor would make the measurements more objective and precise, leading to smaller errors.

In the Kerr effect experiments, while the analysis of the squared voltage dependence on the phase shift yielded consistent results (performed a linear relationship), the precision of the applied voltage measurements could be improved. The small voltage changes may have been influenced by slight variations in the instrumental setup. This could explain some of the experimental uncertainties, especially in the Kerr constant calculation. Also, one should consider the history of the PLZT element, as it affects the consistency of the results. Using a more precise voltage source or using a more sensitive voltmeter could improve the measurement accuracy and allow for a clearer correlation between voltage and phase shift. The highest out of all the g-factors value, indicates a larger gyromagnetic ratio of the plant sample.

7 Conclusion

In this investigation, the Faraday and Kerr effects were successfully examined, focusing on the magneto-optical properties of a flint glass and the electro-optic response of a PLZT element. Through the Faraday effect experiment, the magnetic flux density equation as a function of coil current was determined:

$$\overline{B} = 0.0404I + 6.42 \cdot 10^{-3} \tag{7.1}$$

Using this relationship and linear interpolation of the deflection angle to the mean magnetic flux density, Verdet's constants for various wavelengths were calculated:

$$V_{440} = 51.59 \pm 2.04[radT^{-1}m^{-1}] \tag{7.2}$$
$$V_{505} = 31.44 \pm 2.63[radT^{-1}m^{-1}] \tag{7.3}$$
$$V_{525} = 30.96 \pm 1.14[radT^{-1}m^{-1}] \tag{7.4}$$
$$V_{580} = 24.96 \pm 1.51[radT^{-1}m^{-1}] \tag{7.5}$$
$$V_{595} = 21.6 \pm 0.52[radT^{-1}m^{-1}] \tag{7.6}$$

These results demonstrate a clear trend where the Verdet constant decreases as the wavelength increases, which is consistent with the expected behaviour. It indicates a weakening of the magneto-optical effect for longer wavelengths. Additionally, the Kerr effect experiment provided the determination of the Kerr constant for the PLZT element, yielding a value of:

$$K = (9.13 \pm 0.25) \cdot 10^{-10} m/V^2$$

This value falls in a reasonable range of theoretical values for the PLZT material. The material which was used had the Kerr constant $K = 2.7 \cdot 10^{-9} m/V^2$ according to the PHYWE manual (NL, 2002). The deviation from the theoretical value is acceptable since the constant changes for each experiment, and it requires high accuracy measurements. The improvements in measurement precision–such as using optical sensors for more accurate visibility readings when measuring Verdet constant could further reduce errors and improve the reliability of the results. Future work could additionally explore a broader range of wavelengths for the Faraday effect and investigate other materials for the Kerr effect to expand our understanding of these phenomena.

8 Appendix

8.1 Python Interpolated Flux-Position plots

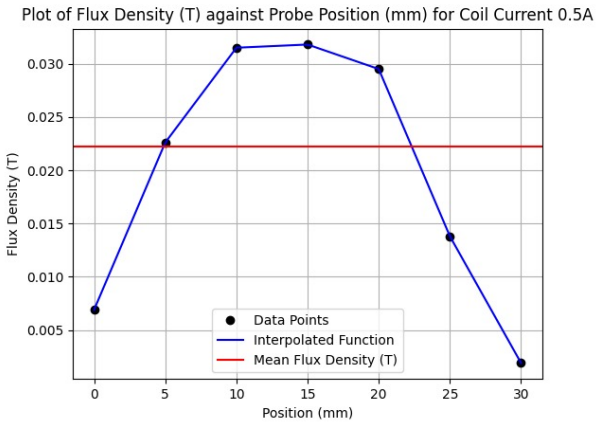

Figure 12: Plot of the Flux Density (T) Against Position (mm) for Coil Current 0.5A

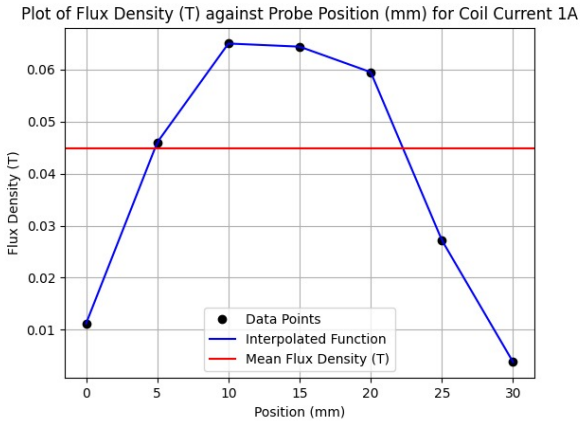

Figure 13: Plot of the Flux Density (T) Against Position (mm) for Coil Current 1A

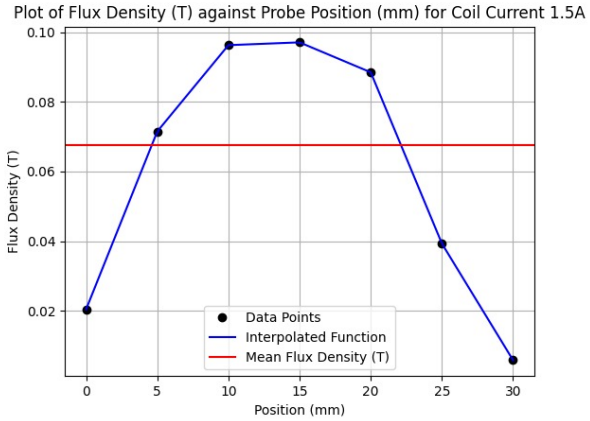

Figure 14: Plot of the Flux Density (T) Against Position (mm) for Coil Current 1.5A

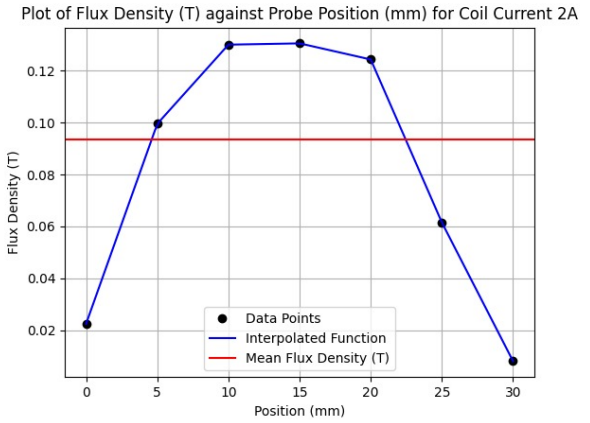

Figure 15: Plot of the Flux Density (T) Against Position (mm) for Coil Current 2A

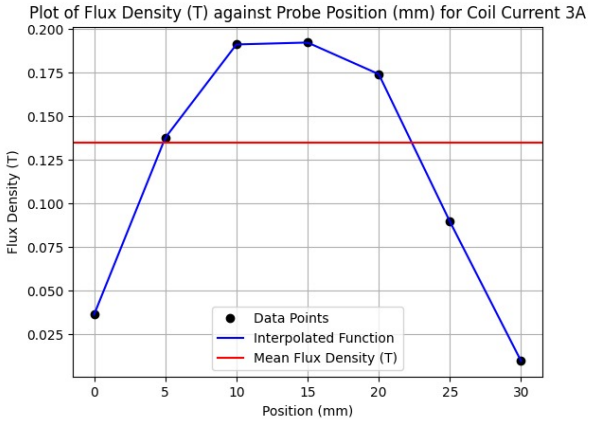

Figure 16: Plot of the Flux Density (T) Against Position (mm) for Coil Current 3A

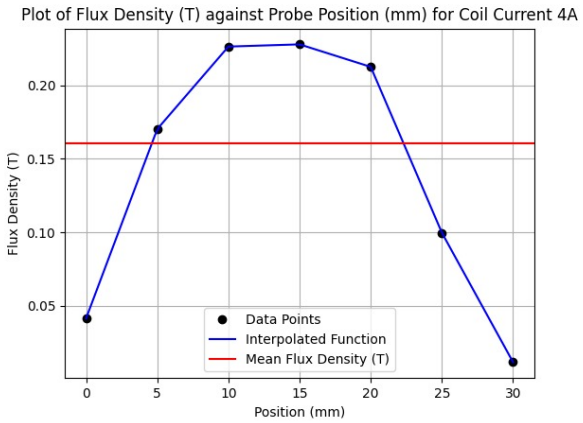

Figure 17: Plot of the Flux Density (T) Against Position (mm) for Coil Current 4A

8.2 Python Code for Numerical Integration

```
# This code was made for the Advanced Physics Lab II Course
# It is used to create an interpolated plot of the of the Magnetic Flux
                                    Density against Position
# And numerically integrate (using the trapezoidal scheme) to find the
                                    mean Flux Density between the rods.

import matplotlib.pyplot as plt
import numpy as np
import scipy
from scipy.interpolate import interp1d


def input_excel_col(string:str):
    arr = []
    print(string)
    while True:
        try: line = float(input().replace('\t',''))
        except EOFError: break
        arr.append(line)
    return np.array(arr)

X = input_excel_col("Input Position (mm):")
Y = input_excel_col("Input Flux Density (T):")
coil_curr = input("Coil Current? (A): ")

f = interp1d(X, Y, kind='linear', fill_value="extrapolate")

L = X[-1] - X[0]
mean_Y = np.trapz(Y, X) / L
```

```
sum_dx2 = np.sum((np.diff(X))**2)

print(f"Mean Flux Density: {mean_Y:.4f} T")

plt.plot(X, Y, 'o', label="Data Points",color='black')
x_fine = np.linspace(min(X), max(X), 100)
plt.plot(x_fine, f(x_fine), '-', label="Interpolated Function", color='
                                    blue')
plt.xlabel("Position (mm)")
plt.axhline(mean_Y, color='red',label='Mean Flux Density (T)')
plt.ylabel("Flux Density (T)")
plt.title(f"Plot of Flux Density (T) against Probe Position (mm) for
                                    Coil Current {coil_curr}A")
plt.legend()
plt.grid()
plt.show()
```

8.3 Graphs of Difference against Flux Density for Different Wavelengths

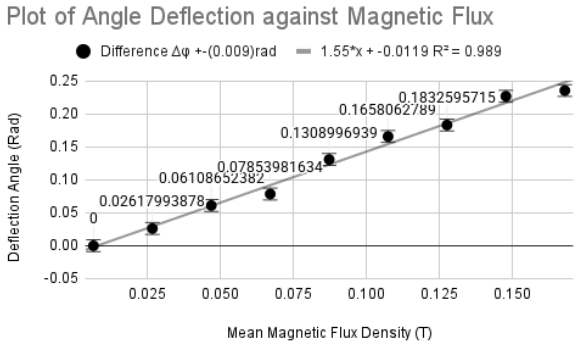

Figure 18: Plot of Angle Deflection against Magnetic Flux Density for Îż=440nm

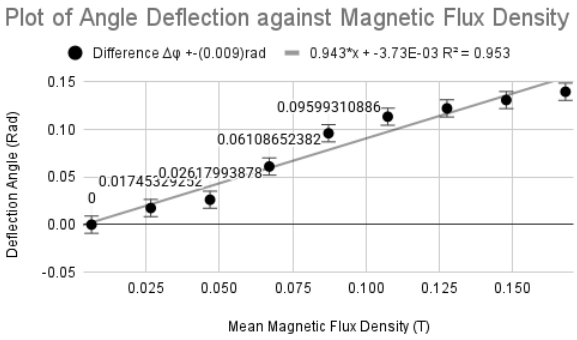

Figure 19: Plot of Angle Deflection against Magnetic Flux Density for Îż=505nm

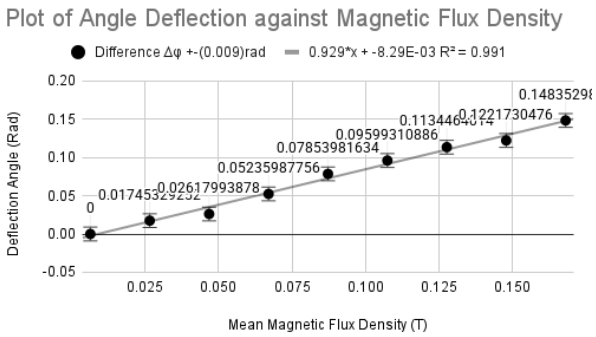

Figure 20: Plot of Angle Deflection against Magnetic Flux Density for Îż=525nm

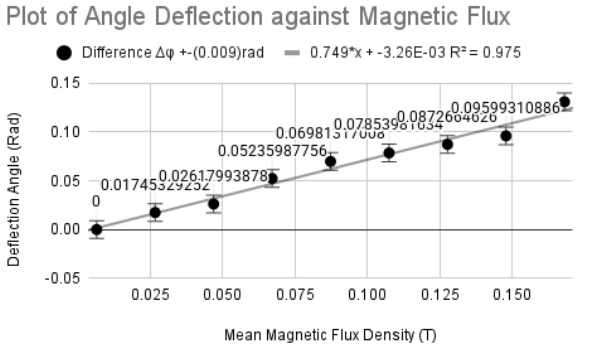

Figure 21: Plot of Angle Deflection against Magnetic Flux Density for Îż=580nm

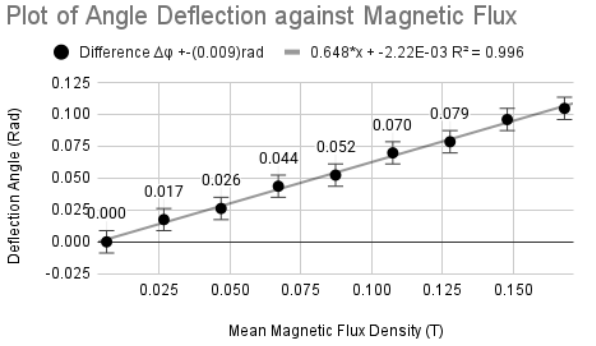

Figure 22: Plot of Angle Deflection against Magnetic Flux Density for Îż=595nm

9 Bibliography

References

Materny, P. D. A., & Mohaghegh, D. F. (2025). Advanced physics lab ii manual. *Constructor University*.

NL, P. (2002). Kerr effect. *Phywe*.